Available online at www.sciencedirect.com
SCIENCE DIRECT®
Journal of Hydrology 298 (2004) 61–79
Journal of Hydrology
www.elsevier.com/locate/jhydrol

Continuous streamflow simulation with the HRCDHM distributed hydrologic model

Theresa M. Carpenter*, Konstantine P. Georgakakos

Hydrologic Research Center, 12780 High Bluff Drive, Suite 250, San Diego, CA 92130, USA

Received 14 May 2003; revised 30 October 2003; accepted 29 March 2004

Abstract

The objective of the authors' work in the area of distributed modeling is to determine the manner with which rainfall input and model parameter uncertainty shapes the character of the flow simulation and prediction uncertainty of distributed hydrologic models. Toward this end and as a tool for the investigation, a distributed model, HRCDHM, has been formulated and tested as part of the NOAA Distributed Model Intercomparison Project (DMIP). This paper examines hourly flow simulations from HRCDHM applied with operational data obtained for the DMIP study watersheds. HRCDHM is a catchment-based, distributed input, distributed parameter hydrologic model. The hydrologic processes of infiltration/percolation, evapotranspiration, surface and subsurface flow (includes leakage to deep groundwater) are modeled along the vertical direction on a subcatchment basis in a manner similar to the Sacramento Soil Moisture Accounting model, and kinematic channel routing carries the flow through the network of subcatchments to the watershed outlet, providing capability for spatially distributed flow simulations. Subcatchment physical properties are derived from various digital terrain and land-characteristics databases through GIS processing and they are used to derive spatially distributed model parameter values. The NWS operational WSR-88D hourly radar rainfall estimates (Stage III product with pixel scale of approximately 4 km) constitute the rainfall forcing and a combination of model-derived and observed hourly surface meteorological data are used to produce the potential evapotranspiration forcing. HRCDHM was applied to and was calibrated for five watersheds for the period May 1993 through June 2000. Validation was done with data not used during the calibration period. This application shows that: (a) the HRCDHM, when forced with hourly data, is able to reproduce well the observed hourly streamflow at the outlet of each study watershed; and (b) beyond these outlet locations, HRCDHM is able to reproduce adequately the hourly flows at several interior locations. A companion paper [J. Hydrol. (2004)], in this issue details the use of the model for the characterization of simulation uncertainty within a Monte Carlo framework.

Keywords: Distributed hydrologic modeling; Radar rainfall; Flow simulation uncertainty; Parameter estimation

1. Introduction

The availability of operational precipitation estimates with high spatial and temporal resolution from weather radars and increasing computer power have brought to the fore the question whether

* Corresponding author. Tel.: +1-858-794-2726; fax: +1-858-792-2519.
E-mail address: tcarpenter@hrc-lab.org (T.M. Carpenter).

0022-1694/$ - see front matter © 2004 Elsevier B.V. All rights reserved.
doi:10.1016/j.jhydrol.2004.03.032

distributed hydrologic models can be used for operational flood and flash-flood forecasting. There is a wealth of distributed models formulated with the advent of distributed databases of land-surface and soils characteristics, following the early paradigm of process-based modeling of Freeze and Harlan (1969). Recently, Carpenter et al. (2001); Ogden et al. (2001); Beven (2002) and Smith et al. (2004, this issue) provide an overview of distributed hydrologic modeling and the issues surrounding its possible use for operational forecasting. It is apparent that the significant influence of rainfall input uncertainties and model structure and parameter errors on small scales have hindered the early utilization of distributed models for operational purposes. Nevertheless, distributed models promise to provide additional information and insight regarding hydrologic conditions at locations without existing streamflow observations (where current operational flow forecasts are made). The NOAA-sponsored Distributed Model Intercomparison Project (DMIP) provided a forum to explore the applicability of distributed models using operational quality data and to elicit issues surrounding their use (Smith et al., 2004, this issue; Reed et al., 2004, this issue).

DMIP focused on several watersheds in the southern Central Plains of the United States. The Illinois River (at Watts and Tahlequah, OK), Baron Fork (at Eldon, OK), and Elk River (at Tiff City, MO) basins are adjacent to one another located in parts of Oklahoma, Arkansas and Missouri. The Blue River at Blue, OK, is an elongated basin located in south-central Oklahoma (see Smith et al., 2004, this issue, for further discussion on DMIP basin selection). This paper discusses the application of the distributed model HRCDHM (Carpenter et al., 2001) to these watersheds as part of DMIP. HRCDHM is a catchment-based, distributed input, distributed parameter model. Subcatchments of a given watershed of interest and their physical characteristics are defined to a specified resolution through GIS processing of digital terrain, soils and land use databases. Hydrologic processes, including runoff generation and channel flow routing, are modeled at the subcatchment level. The modeling philosophy in HRCDHM is guided by the intended purpose of the model, which is the investigation of the effects of rainfall input and parametric uncertainty on the uncertainty of simulated spatially distributed stream flows (e.g. Carpenter et al., 2001). The hydrologic model components of HRCDHM are adaptations of existing operational models and utilize the significant national databases of estimated parameters and soil moisture time series from the current operational spatially lumped models as initial estimates for model parameters and states.

Section 2 provides a brief description of the formulation of HRCDHM components. A discussion of the calibration effort is in Section 3 for all application basins. Section 4 presents our simulation results for the DMIP test watersheds. It is shown that HRCDHM reproduces well the observed hourly flows at the outlet locations of each watershed along with those at several interior locations that were not used during the calibration process. A companion paper (Carpenter and Georgakakos, 2004, this issue) details the use of the HRCDHM model for the characterization of simulation uncertainty within a Monte Carlo framework.

2. Model description

HRCDHM is a spatially distributed parameter and input model. The units that make up the model spatial elements are (irregular) subcatchments, rather than regular grids or TINs. Subcatchment boundaries and hydrological features of a given watershed are defined through GIS processing of digital terrain and stream segment data. At the subcatchment level, hydrologic processes are modeled along the vertical in an aggregate fashion and the result is spatially aggregated surface and subsurface runoff at the subcatchment scale. The arrival time of this runoff at the subcatchment outlet is derived using constant stream velocities and GIS-derived channel lengths within the subcatchments. A kinematic channel routing model based on a regionalized description of the channel cross-sectional geometry of the stream network for each watershed provides the means by which subcatchment outflow becomes spatially distributed streamflow.

The model description is divided into two parts: (a) a discussion of input data, including the GIS input data and input forcing data; and (b) model components, which includes generation of subcatchment mean areal

precipitation (MAP), soil moisture accounting and subcatchment runoff generation, and flow routing through the subcatchment-to-subcatchment channel network. The description is specific to the present application. Other hydrologic processes, such as snow accumulation and ablation, are included in HRCDHM but were not activated in this study. Carpenter et al. (2001) provide a description of an earlier version of HRCDHM.

2.1. Input data

The input data to HRCDHM includes subcatchment geometric properties, channel network information, and hydroclimatic forcing of precipitation and potential evapotranspiration (PET). The subcatchment properties and channel information are derived by geographic information system (GIS) processing. A particular GIS (GRASS, USACERL, 1993) is used to ingest digital elevation and land-use databases and to delineate subcatchments for each study watershed. For this application, USGS 1:250,000-scale (~90-m resolution) digital elevation model data for the region were input, along with USGS Composite Thematic Grid (CTG) land use data. The GRASS subroutine r.watershed is used to delineated stream networks and subcatchments of a given region of interest. R.watershed defines the stream network and contributing areas based on a two-pass, least cost algorithm (Elschlager, 1990). The particular version of r.watershed used has been modified (customized) to provide specific watershed characteristics useful in hydrologic modeling. In this application, the subbasins within each watershed were first delineated with a low area threshold of 5 km^2. This implies that the basin units defining source or headwater subbasins are 5 km^2 or greater in size. Smaller subbasins may be delineated due to the particular stream topology. These small subbasins are aggregated to subcatchments of size consistent with the model components (several tens to hundreds of km^2) based on HRCDHM-user input. This input is a maximum area threshold for the subcatchments of the distributed model; the small scale (5 km^2) subbasins are aggregated to the subcatchments of the distributed model such that the aggregated subcatchments do not exceed the specified area. This two-step delineation process allows for relatively easy modification of the median subcatchment size (i.e. without re-running of the basin delineation process, which can be quite lengthy compared to the hydrologic model processing).

The delineation process provides the model input of aggregated subcatchment geometry, including subcatchment drainage area, average channel slope, stream length, and stream connectivity, which identifies source or headwater subcatchments and internal subcatchments with upstream inflow. This distinction is important for flow routing. For application of HRCDHM to the DMIP watersheds, a single aggregation level for each watershed was used for the modeling. A summary of the aggregated subcatchment properties for the five DMIP watersheds is provided in Table 1. The final subcatchment size chosen for the DMIP application watersheds was determined as a trade-off among achievable spatial resolution (that includes the interior channel points where DMIP validated the simulations), adequacy of area for the estimation of MAP forcing from 4 km-grid radar data, and the ability to generate ensemble simulations for all the watersheds for statistically significant results of uncertainty analysis (Carpenter and Georgakakos, 2004, this issue).

Table 1
Delineation properties of DMIP watersheds

DMIP watershed	ID	Area (km^2)	GIS area (km^2)	Sub-basins	Avg area (km^2)	Avg length(km)	Avg slope
Blue R, blue, OK	BLUO2	1232	1247	21	59.4	10.9	0.008
Elk R, Tiff city, MO	TIFM7	2257	2230	26	85.8	11.6	0.009
Baron fork, Eldon, OK	ELDO2	795	855.6	19	45.0	8.1	0.010
Illinois R, Watts, OK	WTTO2	1644	1589	19	83.6	10.7	0.017
Illinois R, Tahlequah, OK	TALO2	2482	2425	29	83.6	11.9	0.014

The precipitation forcing from historical archives of the operational weather radar (WSR-88D) Stage III product for the region was provided as part of the DMIP datasets. HRCDHM includes a component to ingest the raw binary WSR-88D Stage III product files and store only that portion of the radar coverage window pertinent to the application region. The Stage III product files for the historical period from May 1993 through July 2000 were used. No additional quality control was performed on the radar rainfall data. At each time step, MAP is computed for each subcatchment of the study watersheds based on an arithmetic average of the radar precipitation values for all radar pixels with pixel centroids contained within the given subcatchment. No partial weighting was given to radar pixels with centroids falling outside the given subcatchment. A one-time mapping for each watershed (at the given aggregation level) was made between the radar pixel centroid locations and the delineated subcatchments to identify the pixels contained within each subcatchment. For convenience, the radar precipitation files were processed to compute subcatchment MAP for all delineated subcatchments of each DMIP watershed and for the entire historical record prior to the model simulations.

Another DMIP-provided dataset was energy forcing data from the University of Washington, a 1/8th degree gridded product extracted for grid locations corresponding to the DMIP watershed outlet locations (Maurer et al., 2002; see also the DMIP data description online at http://www.nws.noaa.gov/oh/hrl/dmip/energy_forcing.html). The energy forcing data included model estimates of air temperature, incoming short- and long-wave radiation, atmospheric pressure, vapor pressure, and wind speed computed on the basis of observed surface meteorological data and spatial interpolation procedures. The dataset was used to compute estimates of the potential evaporation rate (derivation given below). The computation was performed outside of the HRCDHM modeling structure and given as input to the hydrologic model components. Accompanying monthly adjustment factors to account for plant type and cover were estimated in the calibration process of the hydrologic model parameters to produce the PET demand for the DMIP watersheds.

2.1.1. Computation of potential evaporation input

The computation of potential evaporation from the energy forcing data follows Penman's combination method (e.g. Chow et al., 1988). In this method, potential evaporation, E_p, over open water surfaces is a weighted sum of a component that is due to energy considerations, E_r, and one that is due to aerodynamic considerations, E_a, such that:

$$E_p = \frac{\frac{4098e_s}{(237.3+T)^2}}{\frac{4098e_s}{(237.3+T)^2}+\frac{C_p p}{0.622\lambda}} E_r + \frac{\frac{C_p p}{0.622\lambda}}{\frac{4098e_s}{(237.3+T)^2}+\frac{C_p p}{0.622\lambda}} E_a \quad (1)$$

where the quantity $4098e_s)/(237.3+T)^2)$ represents the gradient of the saturation vapor pressure curve with respect to temperature [Pa/°C], and $(C_p p/0.622\lambda)$ represents the psychrometric constant [Pa/°C]. The variables of Eq. (1) are defined as follows:

T, air temperature [°C],
e_s, saturation vapor pressure at temperature T [Pa],
C_p, specific heat of air at constant pressure [J/kg/K],
p, atmospheric air pressure [Pa],
λ, latent heat of vaporization of water [J/kg].

The latent heat of vaporization [J/kg] is determined as a function of air temperature [°C] (Chow et al., 1988). The saturation vapor pressure (in mbars or 100 Pa) may be expressed as (Pruppacher and Klett, 1980, p. 625):

$$e_s = a_0 + T(a_1 + T(a_2 + T(a_3 + T(a_4 + T(a_5 + a_6 T))))) \quad (2)$$

for T given in °C. The values of the coefficients are: $a_0 = 6.107799961$; $a_1 = 4.436518521 \times 10^{-1}$; $a_2 = 1.428945805 \times 10^{-2}$; $a_3 = 2.650648471 \times 10^{-4}$; $a_4 = 3.031240396 \times 10^{-6}$; $a_5 = 2.034080948 \times 10^{-8}$; and $a_6 = 6.136820929 \times 10^{-11}$. This relationship applies for the range of water temperature between -50 to $+50$ °C.

Chow et al., (1988, p. 86) give the aerodynamic evaporation component, E_a, of Eq. (1) as:

$$E_a = \frac{0.622k^2}{p\rho_w[\ln(z_2/z_0)]^2}\rho_a u_2(e_s - e_a) \quad (3)$$

where k is the von Karman constant (= 0.4), ρ_a and ρ_w are the densities of air (at temperature T and pressure p) and water, u_2 is the wind velocity at a 2-m height, e_a is the vapor pressure at a 2-m height, $z_2 = 2$ m, and z_0 is the surface roughness height (representative values of surface roughness height are given in Garratt, 1992). Neglecting the contribution of sensible heat and ground heat fluxes, the energy component of evaporation from open water surfaces can be expressed as:

$$E_r = \frac{S_n + L_n}{\lambda\rho_w} \quad (4)$$

where the net radiation [W/m^2] is expressed as a sum of the difference between incoming and reflected solar radiation (S_n) plus the difference between incoming and outgoing long-wave radiation (L_n). The net solar radiation is determined as a function of total shortwave energy input (S_t) and albedo (α):

$$S_n = S_t^*(1 - \alpha) \quad (5)$$

Although albedo is a function of the direction of solar beam, of the proportion of the diffuse radiation and of the land cover, an average value of $\alpha = 0.1$ was assumed. The long-wave energy component (L_n) was computed as the difference in incoming long-wave radiation (L_i) and outgoing long-wave radiation, assuming the outgoing radiation is a function of the surface temperature:

$$L_n = L_i - \{-f\varepsilon\sigma(T + 273.2)^4\} \quad (6)$$

with σ being the Stefan-Boltzmann constant [$= 5.67 \times 10^{-8}$ Wm^{-2} K^{-4}], ε is the emissivity of the surface ($\varepsilon \sim 0.97$ for water), and f is an adjustment factor for cloud cover which was assumed equal to 1.

Assumptions in this derivation suggest application of the estimated potential evaporation on daily time intervals or longer. However, model computations were performed with hourly resolution and the energy forcing dataset was provided with hourly resolution. Therefore a sensitivity analysis was performed to examine the differences in daily potential evaporation based on two computational methods: (a) computation of hourly potential evaporation for daylight hours based on the hourly energy forcing data, which were then combined to give daily values; and (b) computation of average daily values of the energy forcing data which were subsequently used to compute daily potential evaporation values. The energy forcing data provided the hourly input estimates of air temperature, T in [°C]; incoming short-wave radiation, S_t in [W/m^2]; incoming long-wave radiation, L_i in [W/m^2]; atmospheric pressure, p in [kPa]; atmospheric vapor pressure, e_a in [kPa], wind speed, u_2 in [m/s]. The computations were done for the Watts, Blue and Tiff City locations. As an illustration of these differences, the average daily potential evaporation values for all months from the two methods are shown for the Watts location in Fig. 1. For reference, the mean monthly values of observed daily pan evaporation for Eufaula Dam are also shown.

Hourly estimates of potential evaporation were used as input to HRCDHM, rather than the daily values with an assumed diurnal variation cycle. The computed potential evaporation values for the Watts location were assumed representative for the adjacent DMIP watersheds (Watts, Eldon, Tahlequah, and Tiff City). The hourly potential

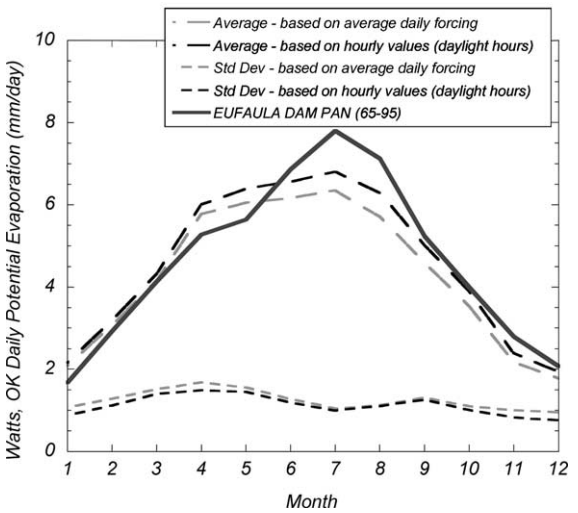

Fig. 1. Comparison of monthly averaged potential evaporation rates (mm/day), computed from DMIP-provided energy forcing fields, with pan evaporation for the Illinois River at Watts, OK.

evaporation values are read by HRCDHM and applied uniformly to all subcatchments within each watershed.

2.2. Hydrologic model components

HRCDHM is a continuous simulation model cast in a form of a set of ordinary differential equations for the subcatchment and channel network. The equations are integrated each hour when new input is available using a numerical integration algorithm with variable integration time step, dependent on the precipitation amount. This section describes the model components employed in this application. These include subcatchment soil moisture accounting, time distribution of surface and subsurface runoff volume in subcatchments, and channel flow routing in the river network of each watershed.

The fundamental structure of the Sacramento soil moisture accounting model (e.g. as expressed in continuous form by Georgakakos, 1986) is employed for each subcatchment to update the soil moisture content of two soil zones over a nominal soil depth of 1 m or so, and to convert input MAP and PET forcing to surface and subsurface runoff. In particular, a rate and state dependent percolation function formulation and an auxiliary surface runoff production mechanism are used to transfer water from the upper to the lower zone and allow the generation of surface runoff as a hybrid infiltration-excess and saturation-excess process. Although the model simulates vertical water transfers and aggregates these within each subcatchment, the area that is saturated near the subcatchment channels is allowed to vary with time giving the model a spatially varying character. The US National Weather Service uses the Sacramento model, in its discrete form (Burnash et al., 1973), for operational flow forecasting in watersheds of area O(1000 km^2). A comprehensive discussion of the physical basis of the model and of methods for parameter estimation is by NOAA (1999).

The general formulation of the model for a single subcatchment may be expressed as:

$$\frac{\partial \underline{X}(t)}{\partial t} = f(\underline{X}(t); \underline{u}(t), \underline{\alpha}) \tag{7}$$

with initial condition $\underline{X}_0$at the initial time, and where $\underline{X}(t)$ represents the vector of model states at time t, $\underline{\alpha}$ is the parameter vector, and $\underline{u}(t)$ represents the vector of MAP and PET input for the subcatchment at time t. The model parameters are listed and described in Table 2 for easy reference, and Section 3 below describes the estimation of the model parameters from hydrometeorological and soils data. Initial conditions, $\underline{X}_0$, for the model states for all subcatchments in a given DMIP watershed were estimated as follows: (a) the lumped parameter model version was run for the period of interest using the hourly resolution, spatially aggregated MAP and PET input; (b) the climatology of the fractional contents of the model soil zones was estimated for each model element from these runs for the record of interest by 5-day periods; (c) the initial fractional contents of the distributed model soil zones for all subcatchments within a watershed were set equal to the appropriate climatological fractions for the initial time; and (d) the distributed model was run through an initial spin-up period (months) with distributed MAP input to reach a stable initial condition for the simulation runs for each case. Given MAP and PET subcatchment input, integration of the subcatchment model Eq. (7) generates estimates of soil water content in the two soil zones considered by the model, surface and subsurface runoff volume, and evapotranspiration for the subcatchment under consideration.

Table 2
Description of Sacramento model parameters

Parameter	Description
x_1^0	Upper zone tension water capacity (mm)
x_2^0	Upper zone free water capacity (mm)
x_3^0	Lower zone tension water capacity (mm)
x_4^0	Lower zone primary free water capacity (mm)
x_5^0	Lower zone secondary free water capacity (mm)
d_u	Upper zone drainage coefficient (interflow) (1/h)
d_l'	Lower zone primary drainage coefficient (1/h)
d_l''	Lower zone secondary drainage coefficient (1/h)
ε	Constant factor in percolation function
θ	Exponent in percolation function
p_f	Fraction of percolation assigned to lower zone free storage
μ	Parameter of base flow not appearing as channel flow
$\beta 1$	Additional impervious area as tension water filled
$\beta 2$	Percent of permanently impervious area

There are two types of routing processes within HRCDHM. The first time-distributes the runoff volume generated in each subcatchment by the soil water model and accounts for the within catchment stream network (upland routing). The second generates flow in the stream network that connects various subcatchments within a single watershed and represents flow through the main stem river network (channel flow routing). For upland routing, a linear reservoir model was used to convert runoff volume into streamflow at the subcatchment outlet. The formulation is given in the form of a cascade of two linear reservoirs (e.g. Georgakakos and Bras, 1982):

$$\frac{dS_1}{dt} = u_c(t) - \alpha_u S_1(t) \tag{8}$$

and

$$\frac{dS_2}{dt} = \alpha_u S_1(t) - \alpha_u S_2(t) \tag{9}$$

where $u_c(t)$ is the runoff volume, $S_j(t)$ is the water storage in the jth reservoir, and α_u is the common parameter. The inverse of α_u represents the time delay associated with each linear reservoir and was defined differently for source (headwater) subcatchment, where the upland flow routing is along the main stem stream length to the subcatchment outlet, and internal subcatchments, where the upland flow feeds the main stem stream collected laterally along the main stem length. The parameter, α_u, is given by (in units of h^{-1}):

$$\alpha_u = \beta_1 V_{source}/L; \quad \text{for source basins} \tag{10}$$

or

$$\alpha_u = \beta_2 V_{lateral}/(A_i/L_i); \quad \text{for internal basins} \tag{11}$$

where β_1 and β_2 are constants for unit conversion; A_i, subcatchment drainage area; L_i, subcatchment main stream length; and V_{source} and $V_{lateral}$ are representative velocities of flows in the main stream of length L_i along the source subcatchment and in a characteristic lateral stream of length (A_i/L_i) across an internal subcatchment. A limited sensitivity analysis with respect to runoff timing was performed to arrive at representative velocity values of 1.25 m/s for source and 0.75 m/s for internal subcatchments, which are consistent with mean velocity estimates for basins with drainage areas of the size of the delineated subcatchments (Leopold, 1994, p. 33).

The channel routing component used in this application is a kinematic routing scheme (e.g. Georgakakos and Bras, 1982). The channel network originates at the outlet of all the source subcatchments and routes water through the length of the main streams of all of the internal subcatchments to the watershed outlet. Each main channel in each subcatchment is divided into a number of reaches for numerical stability of the integration. The water continuity equation for each channel reach is complemented by an equation that approximates the one dimensional momentum equation and gives the discharge of the reach as a monotonic function of the storage in that reach:

$$Q_l(t) = \alpha_{Cl} S_l(t)^m \tag{12}$$

where the l represents a given channel reach, m is a constant exponent, and the parameter α_{Cl} is a function of local stream characteristics (e.g, stream length, slope) and channel cross-sectional characteristics (e.g. shape, roughness) (see Carpenter et al., 2001, for the details of routing formulation). A wide rectangular channel shape is assumed, with a constant roughness coefficient (Morin et al., 2003, have shown little sensitivity in simulated flow to the roughness coefficient in a physically based distributed hydrologic model). Cross-sectional characteristics of top width and hydraulic depth associated with bankfull conditions are defined through regional relationships derived between these cross-sectional parameters and GIS characteristics of the upstream catchment. The relationships used are discussed in Section 3.

3. Model calibration

Given hourly radar precipitation and PET input, along with hourly discharge records for each watershed outlet location, various model component parameters were estimated and/or calibrated for each of the five DMIP watersheds. The calibration approach may be broken into multiple steps which included: (a) development of initial soil model parameters (b) establishment of distributed channel cross-sectional characteristics for each subcatchment

(c) calibration of soil model parameters based on uniformly distributed parameters within each watershed through an interactive calibration procedure, and (d) development of a non-uniform distribution of soil model parameters within each study watershed based on available soil characteristics. Each of these steps is described below.

3.1. Development of initial soil model parameter estimates

Initial estimates for the soil water model parameters were derived from readily available operational and other information on the spatially lumped Sacramento model applications (e.g. Carpenter et al., 2001) for the 1644-km^2 Illinois River at Watts, Oklahoma and the 1232-km^2 Blue River at Blue, Oklahoma. Spatial-scale dependence of the calibrated storage capacities of conceptual hydrologic models and ensuing spatial dependence of model flows due to the spatial variability of precipitation are well documented (e.g. Koren et al., 1999; Finnerty et al., 1997). In the context of distributed hydrologic models, with only a few flow-gauging stations available for calibration, there is a need to develop scale factors to account for spatial rainfall variability effects on the parameter estimates for scales smaller than the scale of calibration. Approximate estimates for such scale factors are developed in the following discussion. In this approximate analysis, the development neglects other contributors to spatial dependence such as the spatial variability of soil column and surface land cover.

For the purposes of this analysis, consider a large catchment of area A_G and an embedded smaller catchment of area A. There is a flow-gauging station at the outlet of the large catchment (location O_G), and calibration of a lumped conceptual hydrologic model of the catchment that includes the soil water capacity as a parameter is desired. Given a time series of hourly mean areal rainfall values over the area A_G and a corresponding time series of hourly flow values for location O_G, an estimate of the soil water capacity x_G of the surface soils, applicable over the large area A_G, may be obtained following standard hydrologic calibration practices. The question is what would this estimate be if this analysis were to be done for the embedded catchment of area $A(< A_G)$ assuming a time series of hourly flows was observed at its outlet (location O). A ratio of the form:

$$\delta = \frac{x}{x_G} \tag{13}$$

is sought, where x denotes the small area (A) estimate of soil water capacity.

A saturation excess mechanism dominating runoff production in these catchments is assumed, with a dry initial condition for the soil column in both catchments. It is reasonable to assume that, given a period of significant rainfall following the initial time, a good calibration procedure would estimate the soil water capacity by the accumulated rainfall volume up to the time when surface runoff will begin. An approximate form of the soil water continuity equation at the catchment scale prior to surface runoff production is:

$$\frac{ds}{dt} = r - e_p \frac{s}{s_o} - \gamma s \tag{14}$$

where r is the rain rate, e_p is the PET demand rate (potential evaporation adjusted for plant transpiration), s_0 is the soil water capacity, and the product (γs) denotes the subsurface flow rate (γ is a constant with units of inverse time). Assuming idealized constant mean hourly rates of rainfall and PET demand during the soil moisture replenishment time, we may integrate the previous equation with initial and final conditions: $s = 0$ at $t = 0$ and $s = s_o$ at $t = T_0$, where T_0 is the time when surface runoff production begins (these times are assumed equal for the small and the large catchments to preserve spatially uniform runoff depth). The result of integration expresses s_0 as a function of the other parameters and input variables:

$$s_o = \frac{r\left(1 - e^{-\left(\frac{e_p}{s_o}+\gamma\right)T_o}\right)}{\left(\frac{e_p}{s_o} + \gamma\right)} \tag{15}$$

For exponent values much smaller than 1 in the numerator of (15), to first order, the relationship simplifies to:

$$s_0 \approx rT_0 \tag{16}$$

This is strictly applicable to cases with significant rainfall volumes over relatively short periods and with small contributions by evapotranspiration and subsurface runoff.

Denoting by p_G (large catchment) and p (small catchment) the MAP rate in the two study catchments and applying (16) in both cases, the following is obtained:

$$\delta \approx \frac{p}{p_G} \tag{17}$$

The ratio (p/p_G) is the area reduction factor for mean areal rainfall and may be estimated by using the relationship of point maximum rainfall to mean areal rainfall (for a variety of empirical formulas, see Bras, 1990, p. 132). Using an empirical formula applicable to areas in the range 20–20,000 km^2 (P_m denotes maximum point rainfall):

$$r = P_m e^{-0.01\sqrt{A}} \tag{18}$$

The scale factor δ for a unique maximum over the study areas is estimated from:

$$\delta = e^{0.01\sqrt{A_G}(1-\sqrt{\varepsilon})} \tag{19}$$

with

$$\varepsilon = A/A_G \tag{20}$$

Fig. 2 shows the variation of factor δ with respect to ε computed for the Watts lumped model area.

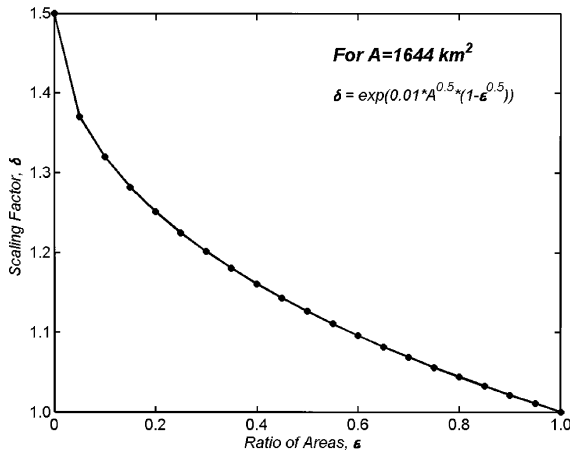

Fig. 2. Illustration of the scaling adjustment factor for soil water model storage capacity parameters based on calibrated lumped model parameters for the Illinois River at Watts, OK.

Table 3
Initial Sacramento model parameter estimates for the DMIP watersheds

Parameter	BLUO2	TIFM7	WTTO2	TALO2	ELDO2
x_1^0	112	103	104	104	110
x_2^0	32	13	15	15	15
x_3^0	118	129	130	130	137
x_4^0	112	103	104	104	110
x_5^0	32	45	45.5	45.5	48
d_u	0.035	0.02	0.02	0.02	0.02
d_l'	0.0005	0.0005	0.0005	0.0005	0.0005
d_l''	0.008	0.008	0.008	0.008	0.008
ε	124.4	75.6	70.8	68.7	72
θ	2.82	2.44	2.39	2.38	2.34
p_f	0.2	0.3	0.3	0.3	0.3
μ	0.0	0.0	0.0	0.0	0.0
β_1	0.0	0.08	0.08	0.08	0.08
β_2	0.05	0.05	0.05	0.05	0.05
Monthly PE adjustment factors					
Jan	1.0	0.45	0.45	0.45	0.45
Feb	1.0	0.40	0.40	0.40	0.40
Mar	1.0	0.40	0.40	0.40	0.40
Apr	1.0	0.50	0.50	0.50	0.50
May	1.0	0.58	0.58	0.58	0.58
Jun	1.0	0.65	0.65	0.65	0.65
Jul	1.0	0.73	0.73	0.73	0.73
Aug	1.0	0.78	0.78	0.78	0.78
Sep	1.0	0.68	0.68	0.68	0.68
Oct	1.0	0.66	0.66	0.66	0.66
Nov	1.0	0.64	0.64	0.64	0.64
Dec	1.0	0.50	0.50	0.50	0.50

Such adjustment factors were computed for the average subcatchment size for each DMIP watershed and applied to the Sacramento model storage capacity parameters to derive uniform initial estimates for these parameters. The initial parameter estimates for the study watersheds are presented in Table 3. The lumped model parameters for the Illinois River at Watts were used to establish initial parameters for the Watts, Tahlequah, Eldon and Tiff City basins. The parameter estimates of the lumped model for Blue River were used for the distributed model application to the Blue River watershed.

3.2. Distribution of channel cross-sectional characteristics

The kinematic routing component requires estimates of the channel cross sections for each

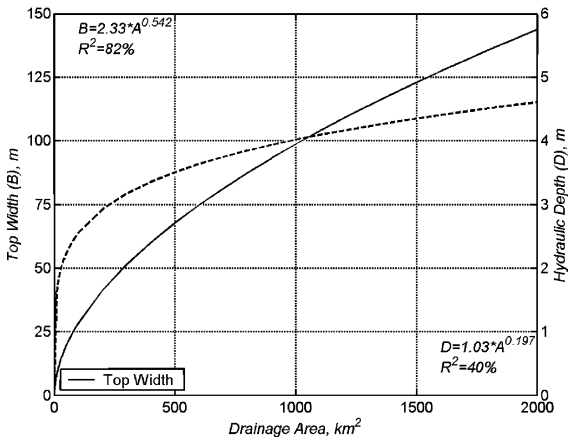

Fig. 3. Regionalized relationships of cross-sectional parameters of bankfull top width and hydraulic depth with subcatchment drainage area.

channel reach. The channel reaches were characterized by properties of interior (i.e. nonhead-water) subcatchments. Estimates of channel bankfull top width and hydraulic depth were produced using regional regression relationships between these parameters and the catchment drainage area. The regional relationships were developed based on stream survey data for a number of streams across Oklahoma (Carpenter et al., 1999) and are depicted in Fig. 3. The coefficients of determination (r^2) reported in this figure indicate that significant variability exists in the stream survey data, and thus there is uncertainty in the channel cross-sectional parameters estimated through these equations. However, without observations at each subcatchment location, these relationships are necessary to compute cross-sectional characteristics for each subcatchment, and to allow for distributed routing parameters within each watershed. Once the relationships were established no other calibration of channel routing model parameters was performed.

3.3. Calibration of uniform soil water model parameters

This step involved establishing a set of calibrated, uniformly applied Sacramento model parameters for each of the study watersheds. Calibration followed the interactive calibration approach outlined by NOAA (1999) and discussed by Smith et al. (2003) The goal of calibration was to have the flow simulation reproduce the observed streamflow at the watershed outlet locations. Input to the calibration included the hourly subcatchment MAP and PET data, along with hourly, observed streamflow for each watershed outlet and the initial parameter estimates discussed earlier. The calibration period was defined as June 1993–May 1999. The sets of calibrated Sacramento model parameters for each watershed are given in Table 4. These parameters were subsequently distributed within each watershed based on soil properties as discussed below. It is noteworthy that due to the process of calibration the changes in the parameter values show very similar trends for all watersheds; that is, upper zone capacities for gravitational free water are increased, while lower zone capacities (both evapotranspiration depleted tension and

Table 4
Final Sacramento model parameter estimates for the DMIP watersheds

Parameter	BLUO2	TIFM7	WTTO2	TALO2	ELDO2
x_1^0	55	110	110	100	80
x_2^0	45	60	45	45	40
x_3^0	210	140	90	90	90
x_4^0	100	70	70	64	45
x_5^0	50	40	45	45	45
d_u	0.04	0.02	0.02	0.02	0.02
d_l'	0.8e-4	0.5e-4	0.0005	0.0004	0.0005
d_l''	0.01	0.005	0.008	0.008	0.008
ε	190	150	60	60	180
θ	3.0	2.8	2.6	2.5	3.4
p_f	0.15	0.35	0.35	0.35	0.35
μ	0.0	0.0	0.0	0.0	0.0
β_1	0.0	0.0	0.01	0.0	0.01
β_2	0.008	0.0	0.03	0.03	0.02
Monthly PE adjustment factors					
Jan	0.30	0.32	0.35	0.30	0.33
Feb	0.32	0.25	0.30	0.30	0.30
Mar	0.35	0.35	0.35	0.35	0.35
Apr	0.35	0.50	0.45	0.45	0.45
May	0.60	0.56	0.57	0.57	0.57
Jun	0.75	0.66	0.66	0.66	0.70
Jul	1.05	0.77	0.77	0.77	0.80
Aug	1.05	0.74	0.74	0.74	0.85
Sep	0.85	0.69	0.65	0.69	0.80
Oct	0.50	0.65	0.63	0.65	0.65
Nov	0.45	0.64	0.63	0.63	0.64
Dec	0.35	0.64	0.63	0.63	0.60

Table 5
Soil-Texture and representative percolation parameter values (interpolates Anderson (1979) results in NWSRFS)

Soil texture classification	ε_R	θ_R
Sand	5.0	1.4
Silty-sand	15.0	1.6
Clayey-sand	25.0	1.8
Sandy-silt	35.0	2.0
Silt	45.0	2.2
Clayey-silt	85.0	2.5
Sandy-clay	125.0	2.8
Silty-clay	165.0	3.1
Clay	205.0	3.5
Unknown/no dominant	45.0	2.2

gravitational free water) are substantially reduced. In most cases, the percolation exponent θ tends to values that are more percolation-limiting and appropriate for higher clay content in soils (see also Table 5 and discussion of next subsection), while the percent impervious area was significantly reduced.

3.4. Spatial distribution of soil model parameters

Additional information on soil characteristics was utilized to define the distribution of soil model parameters after the calibration of uniform parameter values. Specific soil properties were extracted from the STATSGO database (NRCS, 1994) and were related to parameters of the Sacramento model (Table 2). The soil properties were the available water content, permeability, and soil texture classification. The STATSGO database defines these properties for various soils units, component divisions, and depth layers within its coverage. Average soil properties were computed for each subcatchment and for various depth layers consistent with the Sacramento model definition of an upper and lower soil zone based on areal and depth averaging. The distribution of subcatchment model parameters (α_{pi}) was based on a simple scaling of the calibrated parameter values (based on uniform parameters, α_{cal}), by the subcatchment average soil property (S_i) normalized by the average soil property within the watershed ($\overline{S} = \Sigma S_i/N$) :

$$\alpha_{pi} = \frac{S_i}{\overline{S}}\,\alpha_{cal} \tag{21}$$

where i indicates the ith subcatchment of N total within the watershed, and α_{pi} represents one of selected Sacramento parameters. The upper zone storage capacities (free and tension water, x_1^0, x_2^0) were distributed based on the STATSGO available water content property; the STATSGO permeability property was used to scale the interflow rate (d_u). The dominant soil texture classification within a given range of soil depth (20–60 cm) was computed and then associated with representative Sacramento percolation parameters, ε_R and θ_R, for the texture as given in Table 5. Average subcatchment texture-based values were computed and used to scale the calibrated Sacramento model percolation parameters according to Eq. (21). This approach provides a consistent and objective method for distributing model parameters based on observed soil characteristics. As the STATSGO database has national coverage, this method could be applied to any watershed within the United States.

4. Simulation results

With soil water model parameters calibrated based on observed data and distributed to all the subcatchments of each study watershed, HRCDHM was used to simulate streamflow at each watershed outlet and at selected interior points for the historical period, May 1993–July 2000. This section presents the simulation results through statistical summaries for various simulation periods and watershed locations. The historical record was divided into two periods: calibration and validation. The calibration period covers all valid hourly time periods between 6/1/1993 and 5/31/1999. The validation period covers 6/1/1999 through 7/31/2000. Additional results and validation performance measures are given in Reed et al. (2004, this issue).

Figs. 4 and 5 present observed and simulated hydrographs for two watersheds: the Blue River at Blue, OK and the Elk River at Tiff City, MO respectively. The figures show the observed (black line) and simulated (grey line) flows at the outlet of each watershed. The first five panels in each figure present samples of DMIP calibration period events, while the last panel (lower right) presents DMIP validation period events. These figures show that

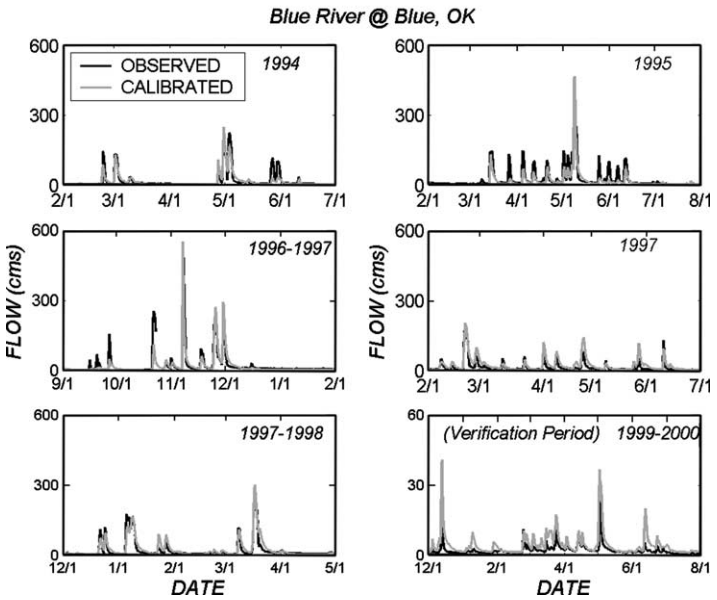

Fig. 4. Hydrograph plot of simulated (gray) and observed (black) flows for the Blue River at Blue, OK. Simulations were performed with the calibrated HRCDHM.

the Blue River watershed response includes more frequent small to medium-sized peaks during periods of activity than the Elk River watershed response (e.g. periods shown in 1995 and 1997). The Blue River watershed stands out in this respect, as the responses of the other study watersheds are similar to the Elk River watershed. Also, during the validation period, only a few significant events occur for the Elk

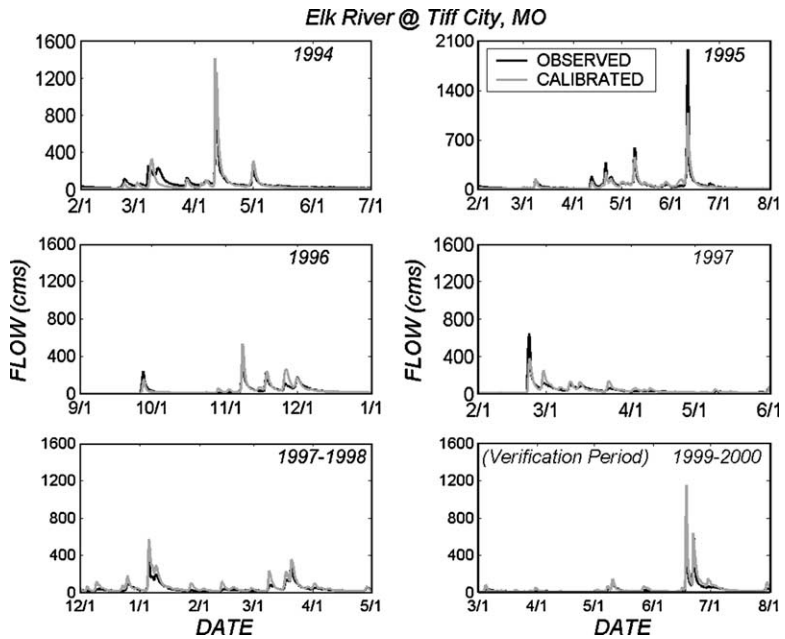

Fig. 5. As in Fig. 4 but for the Elk River at Tiff City, MO.

Table 6
Simulation statistics for watershed outlet locations: uncalibrated run, 6/1993–5/1999

	BLUO2	TIFM7	WTTO2	TALO2	ELDO2
Mean of observations	9.8	28.9	20.9	30.4	11.8
Mean of simulations	4.4	31.1	19.0	28.6	11.6
% Bias	−55.5	7.6	−9.3	−5.8	−1.3
RMS	21.4	57.3	26.9	30.8	17.4
SD, observed	25.2	56.2	35.7	46.9	27.5
SD, simulated	8.3	82.5	43.1	50.9	29.0
Correlation coefficient, r	0.67	0.72	0.78	0.81	0.81
Nash-Sutcliffe efficiency, R^2	0.29	−0.04	0.43	0.57	0.60

River basin, with the largest occurring near the end of the validation period in June 2000. Similar response was seen in the Illinois River and Baron Fork basins. Flows on the Blue River during the validation period are much smaller than during the calibration period (note the change in y-axis scale in Fig. 4), and do not show a significant event during June 2000. In most cases of significant flow for both watersheds, the figures show that the calibrated HRCDHM simulated the timing and the magnitude of the hydrographs reasonably well.

Tables 6 and 7 present summary statistics of each outlet location for the calibration period with (a) initial soil water model parameter estimates (uncalibrated HRCDHM runs) and (b) final parameter estimates (calibrated HRCDHM runs), respectively. The statistics improve significantly with calibration of the soil water model parameters but even for the uncalibrated simulations, HRCDHM produces flow rates of acceptable efficiency (Nash-Sutcliffe efficiency coefficients, R^2, greater than 0.4) for all cases but for Blue River and Elk River, where high negative bias and large simulated variability result in low performance scores (Nash-Sutcliffe efficiency of less than 0.3). After calibration, in all cases the Nash-Sutcliffe efficiency is greater than 0.63 due to significant bias reduction (less than 3% absolute bias) and high reduction of simulation residual variance.

Fig. 6 shows a scatter-plot of the observed versus simulated (calibrated run) hourly flows for each outlet location during the calibration period. The flow values in this figure were sampled every 6 h to reduce the number of points included. Generally, there is good agreement between the simulated and observed hourly flows. The simulation statistics for the calibrated run indicate that HRCDHM is able to reproduce the observed hourly flows at each outlet consistently with small bias and high correlation, explaining more than 60% of the hourly flow variance in all cases.

Similarly, Fig. 7 presents the simulated versus observed hourly flows for the validation period. Although covering a much shorter time period, the results are similar to those presented in Fig. 6. The summary statistics for the validation period are

Table 7
Simulation statistics for watershed outlet locations: calibrated run, 6/1993–5/1999

	BLUO2	TIFM7	WTTO2	TALO2	ELDO2
Mean of observations	9.8	28.9	20.9	30.4	11.8
Mean of simulations	9.9	29.0	20.4	30.9	12.1
% Bias	1.0	0.19	−2.5	1.8	2.8
RMS	14.4	34.0	18.3	23.5	13.4
SD, observed	25.2	56.2	35.7	46.9	27.5
SD, simulated	24.0	57.9	36.4	49.1	25.9
Correlation coefficient, r	0.83	0.82	0.87	0.88	0.88
Nash-Sutcliffe efficiency, R^2	0.68	0.63	0.74	0.75	0.76

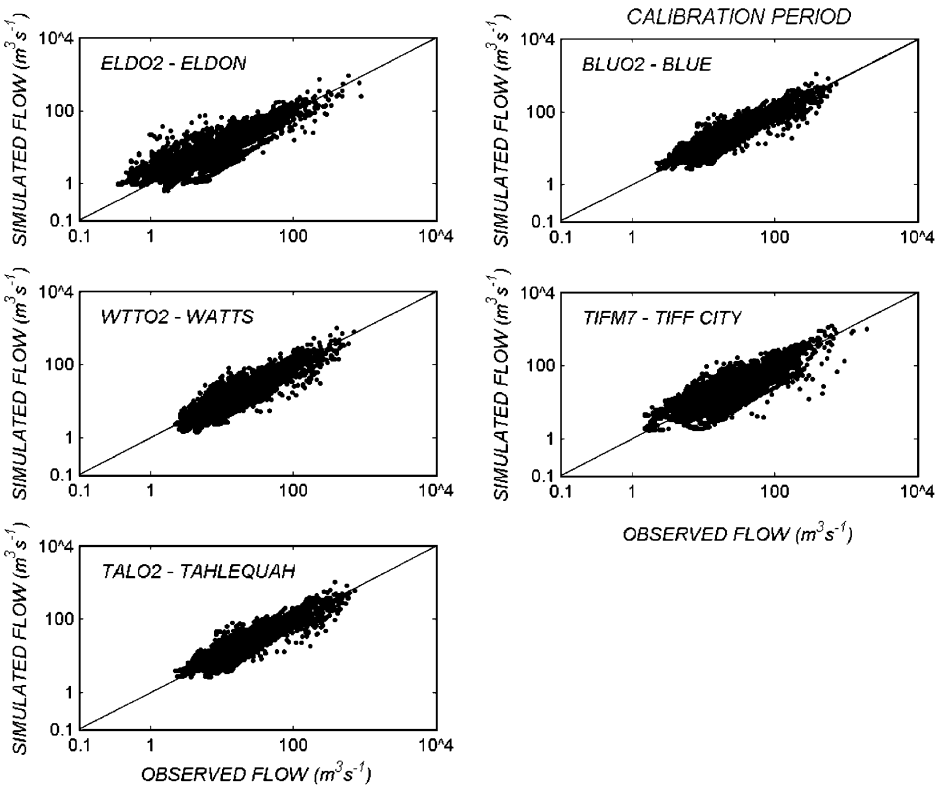

Fig. 6. Simulated versus observed flows (cms) at each DMIP watershed outlet location for the calibration period.

included in Table 8. With the exception of the Blue River (BLUO2) and possibly the Elk River (TIFM7), the overall statistics during the validation period remain good. There is an increase in bias for all basins, but the correlation and Nash-Sutcliffe efficiency coefficients remain high for all but the Blue River. As noted, the flows observed in that watershed during the validation period are in a very low flow regime and the model carries a significant positive bias throughout the simulation (with reasonably high hourly correlation to observed flows) that is responsible for the poor performance measures. The mean observed flow at Blue for the validation is about a fourth of the mean flow observed for the calibration period, and the peak flow for Blue during the validation period is approximately 1/10th of the peak flow observed during the calibration period (see Fig. 4).

Fig. 8 presents the mean monthly flow and standard deviation of the monthly flows for each watershed outlet computed over the calibration period. The mean simulated flows reproduce the mean observed flows quite well for all locations. Greatest differences (albeit small in absolute value) in mean flows occur during the fall months when flows are relatively low and particularly for the Eldon, Tiff City and Tahlequah locations. The differences in simulated and observed standard deviations are largest for the Tiff City and Blue locations, and again during the fall months for Blue. Similar patterns are seen during the validation period, although the record for that is small to draw any hydro-climatologically valid conclusions.

In addition to the outlet locations, along the Illinois River there were several interior locations with observed streamflow data. These include: Flint Creek at Kansas, OK, tributary to the Illinois River and subcatchment of the Tahlequah watershed (with a drainage area at gauge of 285 km^2); the Illinois River at Savoy, OK, a subcatchment of both the Tahlequah and Watts watersheds (with a drainage area of

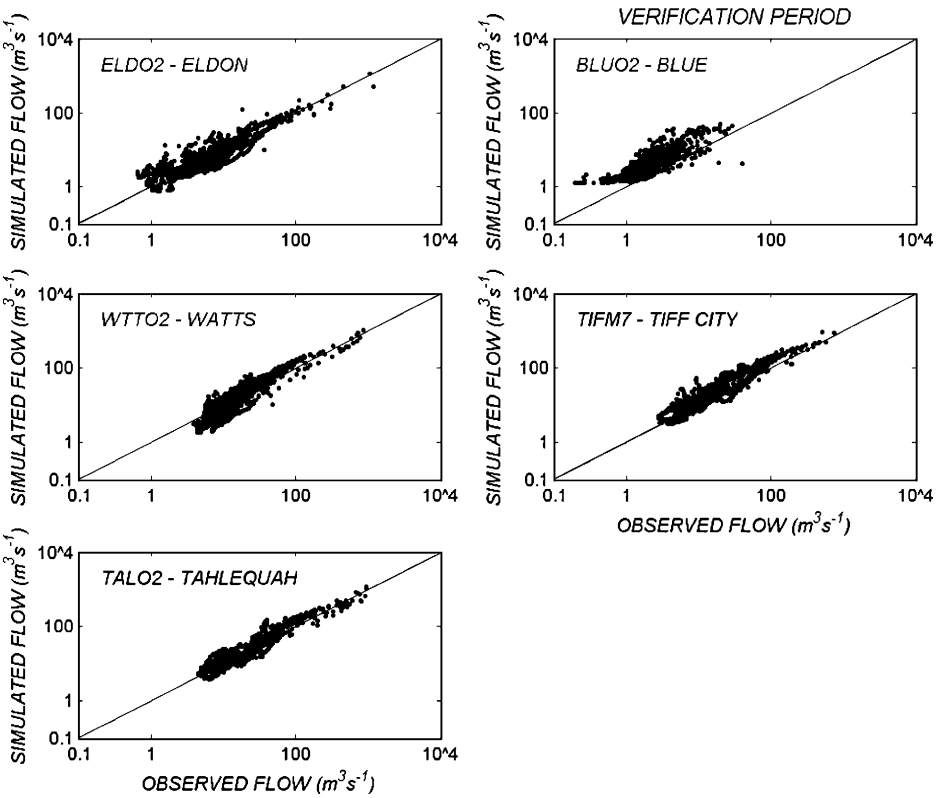

Fig. 7. Simulated versus observed flows at each DMIP watershed outlet location for the validation period.

432 km^2); and the Illinois River at Watts is a subcatchment of the Tahlequah watershed. The simulation results were produced for each of these locations as well as the outlet locations. Note that simulation performance at these locations was not considered during the calibration process (calibration considered only the streamflow at watershed outlet locations). As further validation of the HRCDHM simulations, summary statistics for the interior locations are presented in Tables 9 and 10 for the calibration and validation periods. Fig. 9 also presents a scatterplot of observed versus simulated flows at these interior locations for the calibration period. The statistics for these interior locations, although slightly

Table 8
Simulation statistics for watershed outlet locations: validation period, 6/1999–7/2000

	BLUO2	TIFM7	WTTO2	TALO2	ELDO2
Mean of observations	2.3	19.1	19.6	31.0	9.6
Mean of simulations	4.3	28.0	20.9	35.1	10.0
% Bias	92.2	46.6	6.8	13.5	4.5
RMS	4.4	25.5	18.0	26.1	18.9
SD, observed	2.6	44.2	56.6	78.9	45.4
SD, simulated	5.5	60.8	59.1	80.7	39.3
Correlation coefficient, r	0.76	0.95	0.95	0.95	0.91
Nash-Sutcliffe efficiency, R^2	−1.9	0.67	0.90	0.89	0.83

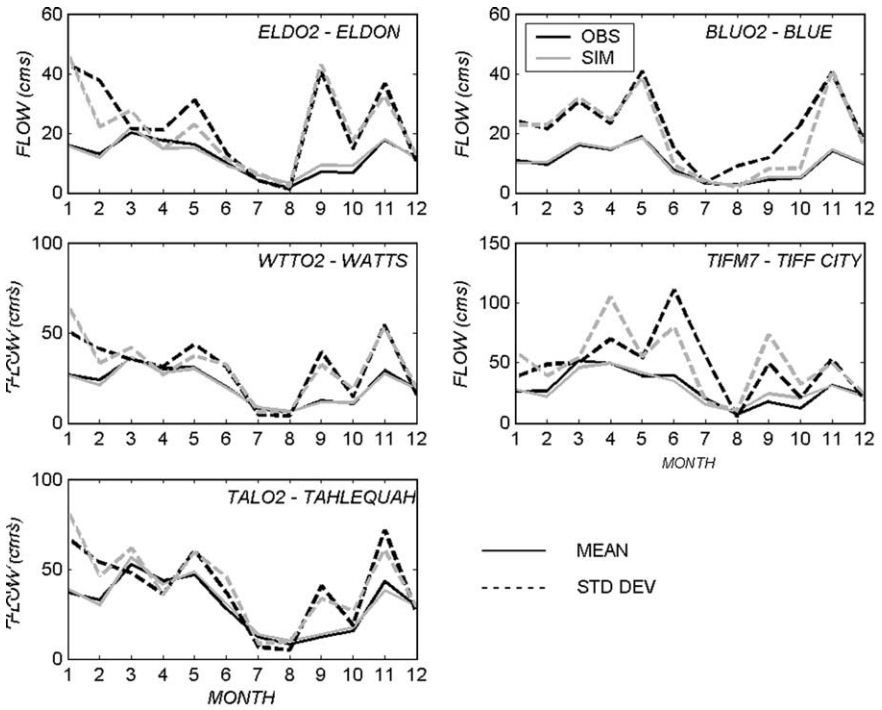

Fig. 8. Monthly means (solid lines) and standard deviations (dashed lines) of simulated (gray) and observed (black) flows for the five DMIP watershed output locations computed for the calibration period.

worse, are comparable to the statistics for the flow simulations at the outlet locations and prove the ability of the distributed model to simulate flows at ungauged interior locations. The average absolute bias is lower than 17%, hourly flow cross-correlation coefficients are 0.8 or greater, and the Nash-Sutcliffe efficiency is at least 0.55 with most cases near 0.7 or greater.

5. Conclusions and recommendations

This paper presents the application of a particular distributed hydrologic model, HRCDHM, for the five Distributed Model Intercomparison Project (DMIP) watersheds. HRCDHM is a catchment-based, distributed input, distributed parameter hydrologic model. Coupling to a GIS system and extensive ingest

Table 9
Simulation statistics for interior locations: calibration run, 6/1993–5/1999

	Savoy (WTTO2)	Watts (TALO2)	Kansas (TALO2)	Savoy (TALO2)
Mean of observations	5.2	20.9	3.3	5.2
Mean of simulations	6.1	20.2	3.5	6.1
% Bias	16.6	−3.3	7.0	17.1
RMS	9.7	18.5	4.0	9.6
SD, observed	16.9	35.7	6.1	16.9
SD, simulated	15.8	36.8	6.4	15.9
Correlation coefficient, r	0.83	0.87	0.80	0.83
Nash-Sutcliffe efficiency, R^2	0.67	0.73	0.57	0.68

Calibration watersheds are shown in parenthesis.

Table 10
Simulation statistics for interior locations: validation period, 6/1999–7/2000

	Savoy (WTTO2)	Watts (TALO2)	Kansas (TALO2)	Savoy (TALO2)
Mean of observations	5.1	19.6	3.9	5.1
Mean of simulations	4.9	21.6	4.3	5.2
% Bias	−2.4	10.3	11.5	3.1
RMS	13.5	20.0	9.1	13.4
SD, observed	24.4	56.6	17.2	24.4
SD, simulated	19.7	59.4	11.6	20.0
Correlation coefficient, r	0.83	0.94	0.87	0.84
Nash-Sutcliffe efficiency, R^2	0.69	0.88	0.72	0.70

Calibration watersheds are shown in parenthesis.

components allow the delineation of user specified arbitrary elementary subcatchment sizes and the ingestion of binary WSR-88D weather radar data for any watershed in the US. A continuous time adaptation of the Sacramento soil water model is used in each elementary subcatchment to produce runoff volume. This volume is distributed in time using subcatchment stream network characteristics and constant stream velocity, and a flow rate is generated at the elementary subcatchment outlet. These flow rates are routed through the channel network using kinematic routing and regionalized estimates of channel cross-sectional properties. Model parameters were spatially distributed to the elementary subcatchments within each study watershed based on available soil and channel

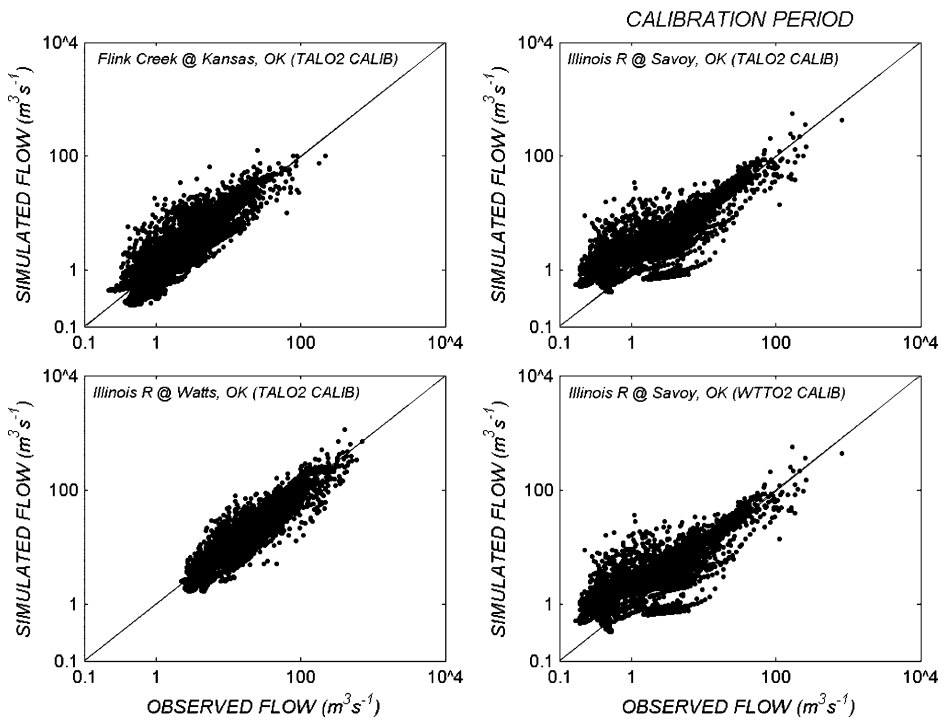

Fig. 9. Simulated versus observed flows at interior subcatchment locations for the calibration period (calibration watershed is given in parentheses).

information. Spatial distribution of the soil water model parameter values is based on the average spatial variation of selected soil properties extracted from the STATSGO soils database for the study watersheds. Channel cross-sectional characteristics of the channel routing component are distributed based on regional relationships between cross-sectional properties with catchment drainage area derived from observed channel survey data for streams in Oklahoma. Given the methods for distributing the parameters of the model components, soil water model parameters for each watershed were calibrated based on observed hourly streamflow records at the watershed outlets.

Evaluation of flow simulations from HRCDHM is presented in terms of summary statistics covering calibration and validation periods. This evaluation shows that with calibration, HRCDHM reproduces well the hourly flows for each of the five watershed outlet locations. In several cases, even without calibration, the distributed model reproduced outlet observed flows with high fidelity. Additionally, evaluation of flow simulation statistics for Illinois River interior locations, not considered during the model calibration process, indicates that HRCDHM is also capable to reproduce well the observed hourly flows at interior ungauged locations (bias less than 17% and Nash-Sutcliffe efficiency values greater than 0.55, with most cases near 0.7 or greater. These results point to the potential of distributed parameter and distributed input models to simulate flows on spatial scales that are smaller than the scales of their calibration.

A significant issue for the application of distributed hydrologic models in operational flow forecasting is the impact of input and parametric uncertainty on the streamflow forecasts. Distributed models, such as HRCDHM, require the estimation of various model parameters at locations without flow, channel, or other observations. Methods for estimating the spatial distribution of both soil model and routing model parameters have been presented in this paper. However, significant uncertainty exists in these estimates for any particular subcatchment. There is also significant uncertainty in precipitation estimates derived from weather radar. These uncertainties influence model simulations significantly on all model output scales, and their analysis is warranted. This uncertainty analysis and results of Monte Carlo sensitivity studies are discussed in the companion paper, Carpenter and Georgakakos (2004, this issue).

A potential future research area associated with the HRCDHM development is to study simulation error dependence on the size of the median subcatchment delineated within the watershed of interest. In addition to more applications for rainfed watersheds but in different topographic regimes, it would also be useful to validate the HRCDHM model simulations in watersheds where snow accumulation and ablation is significant (e.g. Northern US, Rocky Mountain and California Sierra Nevada watersheds). For these cases and especially in mountainous terrain, uncertainty in estimated distributed precipitation is high as weather radar data suffer significant biases (e.g. ground clutter, partial beam filling, etc.). With respect to model reproduction of observed flows, a logical next step is to examine the performance of HRCDHM in true forecast cases when distributed *forecast* input is used to force the model.

Acknowledgements

The research work was sponsored by NOAA Grant No. NA07WH0368. Supplemental support was provided by the California Applications Project of the Scripps Institution of Oceanography, UCSD. The technical support and organizational assistance of the NWS Hydrology Lab Staff, and in particular Michael Smith and Seann Reed, throughout DMIP is greatly appreciated. Jason Sperfslage of HRC assisted with HRCDHM data management issues. The authors are grateful to two anonymous reviewers and Michael Smith, whose comments improved the readability of this paper.

References

Anderson, E., 1979. National Weather Service Office of Hydrology Training Course Handbook. Section entitled Initial soil-moisture parameter estimates by hydrograph analysis, supplement to NWSRFS User's Documentation (http://www.nws.noaa.gov/oh/hrl/nwsrfs/users_manual/htm/formats.htm).

Beven, K., 2002. Towards an alternative blueprint for a physically based digitally simulated hydrologic response modelling system. Hydrol. Process. 16, 189–206.

Bras, R.L., 1990. Hydrology, an Introduction to Hydrologic Science, Addison-Wesley, Reading, Massachusetts, 643 pp.

Burnash, R.J., Ferral, R.L., McGuire, R.A., 1973. A generalized streamflow simulation system: conceptual modeling for digital computers, Technical Report, Joint Federal-State River Forecast Center, US National Weather Service and California Department of Water Resources, Sacramento, CA, 204 pp.

Carpenter, T.M., Georgakakos, K.P., 2004. Impacts of parametric and radar rainfall uncertainty on the ensemble streamflow simulations of a distributed hydrologic model. J. Hydrol. 298(1–4), 202–221.

Carpenter, T.M., Sperfslage, J.A., Georgakakos, K.P., Sweeney, T., Fread, D.L., 1999. National threshold runoff estimation utilizing GIS in support of operational flash flood warning systems. J. Hydrol. 224, 21–44.

Carpenter, T.M., Georgakakos, K.P., Sperfslage, J.A., 2001. On the parametric and NEXRAD-radar sensitivities of a distributed hydrologic model suitable for operational use. J. Hydrol. 254, 169–193.

Chow, V.T., Maidment, D.R., Mays, L.W., 1988. Applied Hydrology, McGraw Hill Publishing, New York, 572 pp.

Elschlager, C.R., 1990. Using the A^T search algorithm to develop hydrologic models from digital elevation data. Unpublished paper, US Army Corps of Engineers Construction Engineering Research Laboratory, Champaign, IL, 7 pp.

Finnerty, B.D., Smith, M.B., Koren, V., Seo, D.J., Moglen, G., 1997. Space-time scale sensitivity of the Sacramento model to radar-gage precipitation inputs. J. Hydrol. 203, 21–38.

Freeze, R.A., Harlan, R.L., 1969. Blueprint for a physically-based, digitally-simulated hydrologic response model. J. Hydrol. 9, 237–258.

Garratt, J.R., 1992. The Atmospheric Boundary Layer, Cambridge University Press, New York, 316 pp.

Georgakakos, K.P., 1986. A generalized stochastic hydrometeorological model for flood and flash-flood forecasting, 1, Formulation. Water Resour. Res. 22(13), 2083–2095.

Georgakakos, K.P., Bras, R.L., 1982. Real-time, statistically linearized, adaptive flood routing. Water Resour. Res 18(3), 513–524.

Koren, V.I., Finnerty, B.D., Schaake, J.C., Smith, M.B., Seo, D.-J., Duan, Q.Y., 1999. Scale dependencies of hydrology models to spatial variability of precipitation. J. Hydrol. 217, 285–302.

Leopold, L.B., 1994. A View of the River, Harvard University Press, Cambridge, MA, 298 pp.

Maurer, E.P., Wood, A.W., Adam, J.C., Lettenmaier, D.P., Nijssen, B., 2002. A long-term hydrologically-based data set of land surface fluxes and states for the conterminous United States. J. Climate 15, 3237–3251.

Morin, E., Georgakakos, K.P., Shamir, U., Garti, R., Enzel, Y., 2003. Investigating the effect of catchment characteristics on the response time scale using distributed model and weather radar information. In: Tachikawa, Y., Vieux, B.E., Georgakakos, K.P., Nakakita, E. (Eds.), Weather Radar information and Distributed Hydrological Modelling, 282. IAHS Publ. 282, International Association of Hydrological Sciences, pp. 177–185.

NOAA, 1999. Calibration of the Sacramento Soil Moisture Accounting Model: Demonstration of an interactive calibration approach. NOAA Video Series, Hydrology Laboratory, National Weather Service, NOAA, Silver Spring, MD, 5-hour VHS Video set and handbook.

NRCS (Natural Resource Conservation Service), 1994. State Soil Geographic (STATSGO) Database, Misc. Publ. 1492, U.S. Dept of Agriculture, Fort Worth, TX, p. 37 + Appendices.

Ogden, F.L., Garbrecht, J., DeBarry, P.A., Johnson, L.E., 2001. GIS and distributed watershed models, II, Modules, interfaces and models. J. Hydrol. Eng. 6(6), 515–523.

Pruppacher, H.R., Klett, J.D., 1980. Microphysics of Clouds and Precipitation, D. Reidel Publishing Company, Boston, MA, 714 pp.

Reed, S., Koren, V., Smith, M.B., co-authors, 2004. Overall distributed model intercomparison project results. J. Hydrol. 298(1–4), 27–60.

Smith, M.B., Seo, D.-J., Koren, V.I., et al., 2004. The distributed model intercomparison project (DMIP): an overview. J. Hydrol. 298(1–4), 4–26.

Smith, M., Laurine, D.P., Koren, V.I., Redd, S.M., Shange, Z., 2003. Hydrologic model calibration in the National Weather Service. In: Qingyun, D., Gupta, H.V., Sorooshian, S., Rousseau, A.N., Turcotte, R. (Eds.), Calibration of Watershed Models, Water Science and Application, vol. 6. American Geophysical Union, pp. 133–152.

USACERL, 1993. GRASS4.1 User's Reference Manual. U.S. Army Corps of Engineers, Construction Engineering Research Laboratories, Champaign, IL, 566 pp.